PCCP

COMMUNICATION

View Article Online
View Journal | View Issue

Cite this: *Phys. Chem. Chem. Phys.*, 2026, **28**, 7835

Received 28th January 2026,
Accepted 3rd March 2026

DOI: 10.1039/d6cp00307a

rsc.li/pccp

Structural and optical responses of molecular solids to swift heavy ion irradiation under high pressures

Jiaxu Liang, *[a] Lkhamsuren Bayarjargal,[a] Ioannis Tzifas,[b] Roman Belikov,[a] Lena Wedek,[a] Christopher Schröck,[ab] David Merges,[a] Kay-Obbe Voss,[b] Pascal Simon,[b] Christina Trautmann,[b] Maria Eugenia Toimil-Molares[bc] and Björn Winkler[a]

We investigated the responses of three representative molecular solids to swift heavy ion irradiation at high pressures. The coupled extreme conditions induce markedly different changes, including polymerization, decomposition, and phase transitions. This synergistic approach offers a promising route for designing novel materials with distinct structures and properties.

Swift heavy ions (SHIs) refer to ions heavier than carbon that are accelerated to kinetic energies in the MeV–GeV range at large accelerator facilities. When traversing a material, each SHI interacts primarily through electronic stopping, with high energy densities being deposited to the target.[1,2] This triggers intense electronic excitation and ionization processes along the ion trajectory on ultrafast timescales ($\sim 10^{-15}$–10^{-13} s).[1,2] The energy stored in the electronic subsystem is subsequently transferred to the atomic lattice *via* electron–phonon coupling, initiating the formation of a cylindrical damage zone, commonly referred to as an ion track.[3,4] Such tracks typically have a diameter of 5–10 nm, while their length depends on the ion energy and the corresponding range in the material. Proposed mechanisms for track formation include local melting (thermal spike), lattice destabilisation and rapid recrystallization.[3,4] The specific response to these extreme excitations depends strongly on intrinsic material properties. Observed physical and chemical modifications include the formation of extended defects, phase transitions, amorphization and chemical reactions along the track. Up to now, most SHI irradiation experiments have been conducted under ambient pressure. The combination of static high pressure and SHI irradiation has been demonstrated to affect the phase behavior of ionic compounds in ways distinct from those induced by pressure or irradiation alone.[5–7]

In contrast to ionic compounds, the constituents of molecular solids are held together by weak intermolecular forces, such as van der Waals interactions and hydrogen bonds.[8] This fundamental distinction in bonding and structure gives rise to significant differences in their physical and chemical behaviors. When subjected to compression, molecular systems may undergo profound transitions from molecular states to extended atomic networks, driven by reduced intermolecular distances and increased overlap of electronic orbitals.[8,9] These changes may give rise to emergent phenomena such as polymerization, metallization, or superconductivity.[8,9] Due to such different characteristics, SHI irradiation at high pressures is expected to induce responses in molecular solids that differ substantially from those observed in ionic compounds.

We investigated irradiation effects by Raman and optical imaging in a series of molecular systems, including carbon monoxide (CO), urea($CO(NH_2)_2$), and sulfur. For the irradiation of pressurized molecular solids in diamond anvil cells (DACs) (Fig. 1), we used a dedicated platform recently installed at a beamline of the heavy ion synchrotron (SIS18) operated by the GSI Helmholtz Center for Heavy Ion Research (Darmstadt, Germany).[10] This approach identifies distinct phenomena such as polymerization, decomposition, or phase transition, and provides a basis for exploring a broader range of molecular systems under the synergistic effects of SHI irradiation and high pressure.

CO has been extensively studied at high pressures because of its ability to transform into a high-energy-density material by polymerization.[11] At pressures below 5 GPa, CO exists as molecular crystals exhibiting three solid phases (β,δ,ε).[12] When the pressure exceeds 5 GPa, molecular CO becomes unstable and begins to transform into polymeric CO (p-CO), consisting of lactone-like carbonyl groups and chains with conjugated C=C bonds.[13]

The mixture of CO and helium at 4.2(2) GPa is used for SHI irradiation experiments. Before irradiation, our CO-helium

[a] *Institute of Geoscience, Goethe University Frankfurt, 60438, Frankfurt, Germany. E-mail: j.liang@kristall.uni-frankfurt.de*
[b] *Materials Research Department, GSI Helmholtz Centre for Heavy Ion Research, Darmstadt, Germany*
[c] *Department of Materials- and Geosciences, Technical University of Darmstadt, Germany*

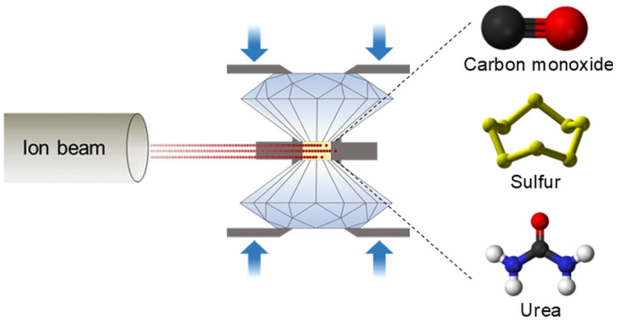

Fig. 1 Simplified scheme of SHI irradiation of molecular solids under high pressure conditions.

sample at 4.2(2) GPa is transparent and colorless with a clearly visible phase separation,[14] as shown in Fig. 2a. The helium bubble enables the identification and monitoring of the CO in the DAC during irradiation. After SHI exposure to a fluence of 3.0×10^{13} ions cm^{-2}, the CO turns dark (Fig. 2a), indicating substantial beam-induced structural modifications. Noticeably, some coloration also appears in the helium bubble, although it is less pronounced than that in the CO solid region. We assume that this originates from colored CO dissolved in helium. *In situ* optical imaging reveals a gradual darkening of both helium and CO areas with increasing ion fluence (Fig. 2c), suggesting that the structural transition during SHI irradiation proceeds in a progressive way rather than an uncontrolled chain mechanism (*e.g.* radical reactions).

Raman spectra before and after SHI irradiation of 3×10^{13} ions cm^{-2} fluence are shown in Fig. 2b. Upon irradiation, the sharp C≡O stretching band at 2140 cm^{-1} observed in the pristine sample disappears completely, and a new broad peak emerges at around 1600 cm^{-1}. This broad Raman feature is characteristic of disordered polymeric carbon–oxygen networks (p-CO) containing conjugated C=C and C=O bonds,[11,13] indicating that the coloration after irradiation results from the transformation of molecular CO into p-CO. For comparison, the CO-helium mixture is compressed to 8.7(3) GPa without irradiation to obtain p-CO by pressure alone. The Raman spectrum of the pressure-induced product (Fig. S1) resembles that of irradiation-induced p-CO. From the optical images, the solid CO region turns yellow, whereas most of the helium region remains colorless (Fig. S2). Our results suggest that SHI irradiation at 4.2(2) GPa can effectively trigger the polymerization of CO, below the typical pressure threshold of above 5 GPa without irradiation. This implies that CO molecules can be effectively activated for bond reconfiguration through SHI-induced electronic excitation, thereby lowering the pressure threshold to overcome the thermodynamic barrier. Further experiments at lower pressures are expected to elucidate the minimum pressure at which SHI irradiation can initiate CO polymerization. The simultaneous application of pressure and ion irradiation offers an alternative pathway for synthesizing high-energy-density carbon–oxygen materials.

Urea is one of the most common nitrogen-containing organic compounds in the Earth's shallow crust.[15] Unlike CO, where the molecules are bound to each other by van der Waals interactions, urea forms a three-dimensional network in which the molecules are linked by N–H···O hydrogen bonds. High pressure can alter the strength and geometry of these hydrogen bonds, thereby inducing multiple phase transitions in the sequence I–III–IV–V at respective pressures of 0.5 GPa, 3.0 GPa and above 7.0 GPa according to the literature.[16–18] As the nomenclature of urea phases is inconsistent in the literature, we follow the phase naming adopted in these papers.[17,18]

Two DACs were loaded with urea samples, and subsequently pressurized to 1.1(2) GPa and 7.1(3) GPa, respectively. After irradiation up to fluence of 2.3×10^{12} ions cm^{-2} at 1.1(2) GPa, the sample turns yellow-brown (Fig. S3), whereas its color remains nearly unchanged up to 3.4×10^{12} ions cm^{-2} at

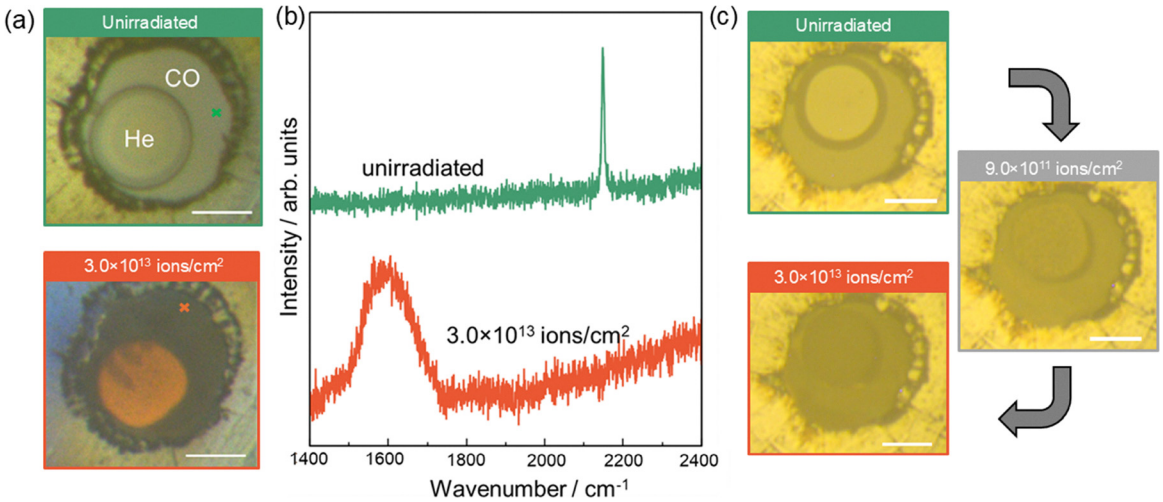

Fig. 2 CO at 4.2(2) GPa before and after ion irradiation with 3.0×10^{13} ions cm^{-2}. (a) Off-line optical images of CO-helium mixture before (top) and after (bottom) irradiation; (b) Off-line Raman spectra of CO before (top) and after (bottom) irradiation; (c) *In situ* optical imaging of CO during irradiation. The '*x*' marks in (a) indicate a representative off-line Raman measurement point from which the spectra in (b) were obtained. The scale bar is 50 μm.

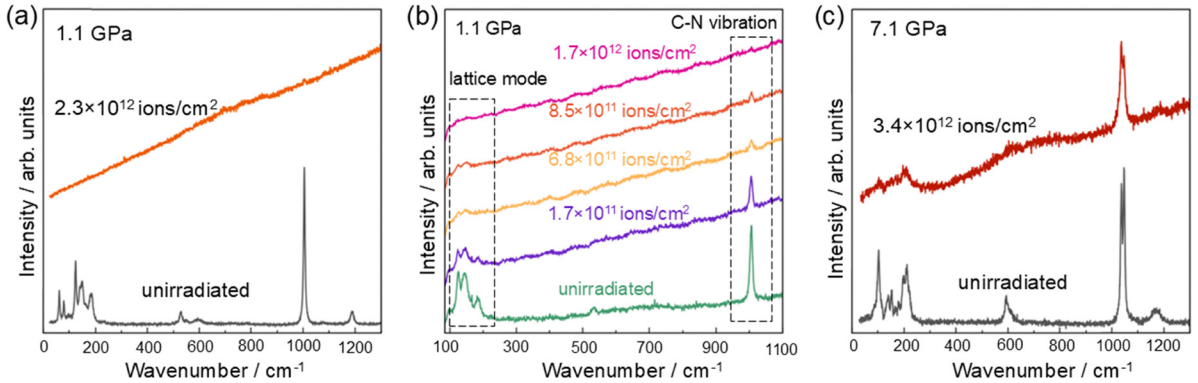

Fig. 3 Raman spectroscopy of urea upon SHI irradiation at 1.1(2) GPa with fluence up to 2.3 × 10^{12} ions cm^{-2} and at 7.1(3) GPa with fluence up to 3.4 × 10^{12} ions cm^{-2}. (a) Off-line Raman spectra at 1.1(2) GPa before and after irradiation; (b) *In situ* Raman spectra at 1.1(2) GPa during irradiation; (c) Off-line Raman spectra at 7.1(3) GPa before and after irradiation.

7.1(3) GPa. The UV-Vis spectra (Fig. S4) show that the sample irradiated at 1.1(2) GPa exhibits a pronounced shift towards longer wavelengths relative to that at 7.1(3) GPa, consistent with the observed color difference in Fig. S3. This red shift indicates a greater π-conjugation length arising from a higher degree of aromatization.[19]

The Raman spectrum collected before irradiation at 1.1(2) GPa (Fig. 3a) exhibits the characteristic sharp peaks of crystalline urea in phase III,[16] including lattice modes in the low-frequency region (<200 cm^{-1}), weak C–N bending modes near 500–600 cm^{-1}, and prominent C–N stretching modes at ~1000 cm^{-1}. SHI irradiation with fluence of 2.3 × 10^{12} ions cm^{-2} at 1.1(2) GPa results in a complete loss of sharp peaks, producing a featureless fluorescent background indicative of significant structural modifications. The corresponding fluorescence spectrum (Fig. S5) displays a broad emission band from 500 to 850 nm centered at 660 nm with no detectable Raman modes. The fluorescence characteristics match those of urea decomposition products formed upon heating, namely nitrogen, oxygen-contained carbon nanodots composed of various molecular fluorophores.[20] Thus, we infer that SHI irradiation induces decomposition of urea at 1.1(2) GPa. The *in situ* Raman spectra of urea recorded during SHI irradiation at 1.1(2) GPa (Fig. 3b) reveal a gradually increasing fluorescence background accompanied by an intensity decrease of Raman bands associated with C–N vibrations (at ~1000 cm^{-1}).

The Raman spectrum of urea at 7.1(3) GPa before irradiation (Fig. 3c) corresponds to the phase IV[16] with a denser molecular packing and reorganization of the N–H···O hydrogen-bond network into a more heterogeneous configuration,[16,17] evidenced by the featureless N–H modes in 3200–3400 cm^{-1} range (Fig. S6). After irradiation at 7.1(3) GPa with fluence 3.4 × 10^{12} ions cm^{-2}, the Raman peaks of urea are still present despite the fluorescent background. The sharp C–N stretching band near 1040 cm^{-1} shows a slight broadening, accompanied by a featureless C–N bending band at 600 cm^{-1}. The N–H modes in 3200–3400 cm^{-1} are no longer detectable due to the fluorescent background. The lattice modes below 300 cm^{-1} decrease in intensity and become more or less featureless, indicating partial disordering or amorphization of the urea crystal.

The pressure dependence of the SHI-induced degradation in urea is of particular interest for the production of nitrogen-containing carbon materials, as it offers insights into how materials can be tailored through controlled design and synthesis conditions. The different molecular packing at different pressures may contribute to this pressure-dependent phenomenon because structural and thermal properties of the material could affect the energy transfer from the electronic to the atomic subsystem in multiple ways.[2] However, additional data across a wider range of beam and pressure parameters will be required in future experiments to elucidate the mechanisms.

In contrast to compounds such as CO and urea, sulfur is a monoatomic molecular solid. It exhibits a diversity of allotropes, including a wide range of cyclic and chain-like molecular forms.[21] At ambient pressure, sulfur primarily exists as cyclic S_8 molecules, with the most stable phase being orthorhombic α-S_8 (S-I). Under high-pressure high-temperature conditions, sulfur undergoes a series of phase transitions, forming multiple solid phases,[22] including monoclinic β-S_8 and rhombohedral S_6 (S-IV) with cyclic molecules, as well as trigonal (S-II) and tetragonal (S-III) phases composed of chain-like molecules.

The sulfur crystals are compressed in two DACs, together with the urea samples, to 1.1(2) GPa and 7.1(3) GPa, respectively. At 1.1(2) GPa, the initially nearly transparent sample develops a pronounced yellow coloration (Fig. S8). The UV-Vis absorption spectrum (Fig. S7) shows a steep absorption edge at around 450 nm, consistent with the observed yellow appearance. Before irradiation, the Raman spectrum at 1.1(2) GPa exhibits the characteristic peaks of orthorhombic α-S_8,[23] dominated by the symmetric S–S stretching mode at ~475 cm^{-1} and a symmetric S–S–S ring-bending mode in the range of 120–300 cm^{-1} (Fig. 4a). Several weaker modes are also observed below 120 cm^{-1}, consistent with the known lattice mode of α-S_8.[23] After SHI irradiation at 1.1(2) GPa, the peaks associated with lattice and S–S–S bending modes (<300 cm^{-1}) appear on an enhanced background. The dominant S–S stretching band at 475 cm^{-1} becomes broader and more asymmetric. These changes indicate that the long-range crystalline order of orthorhombic α-S_8 is partially destroyed.[21,23,24]

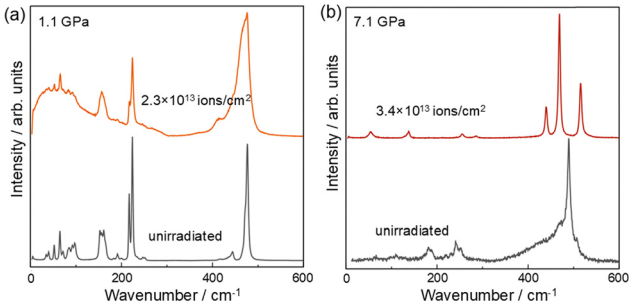

Fig. 4 Off-line Raman spectroscopy of sulfur before and after SHI irradiation at 1.1(2) GPa (a) with fluence up to 2.3×10^{12} ions cm^{-2} and at 7.1(3) GPa (b) with fluence up to 3.4×10^{12} ions cm^{-2}.

The optical images (Fig. S7) collected at 7.1(3) GPa before and after irradiation reveal a color change from yellow to dark red, which is a well-known signature of the transition from ring-like S_8 molecules to chain-like sulfur structures.[21,25] This darkening indicates that SHI irradiation induces ring opening and formation of polymeric chain sulfur. At the higher pressure of 7.1(3) GPa before irradiation, the sharp peak at 489 cm^{-1} (S–S stretching) and small peaks in the 150–280 cm^{-1} range (ring-bending modes) suggest that S_8 rings still exist at this pressure. The broad band between 300 and 600 cm^{-1} is characteristic of chain-like sulfur molecules due to fast compression.[22,26] These features indicate that sulfur at 7.1(3) GPa consists of an amorphous mixture of S_8 rings and chain-like sulfur species. After SHI irradiation at 7.1(3) GPa, three prominent sharp peaks appear at 440, 469, 516 cm^{-1} assigned to S–S stretching modes of the S-II phase,[21] a clear signal for a transformation from molecular S_8 rings to an ordered, triangular-chain high-pressure phase (S-II).[21,25]

These results demonstrate that SHI irradiation in combination with pressure efficiently breaks S_8 rings and drives the system toward a more ordered polymeric chain-like structure, which is thermodynamically stable above 400 °C in the pressure range of 2–10 GPa.[21] Chain-like sulfur materials are considered promising for applications in diverse fields, including optoelectronic devices, energy-storage batteries, and infrared functional materials.[22] Our results suggest a potential pathway for the formation of novel chain-structured materials.

Pressure can drive materials toward new thermodynamic equilibrium states by fundamentally altering their physical and chemical bonding.[9,27] However, kinetically controlled techniques are frequently required to accelerate the transformation.[27] Our results demonstrate that SHI irradiation offers an alternative way of manipulating kinetic pathways in molecular solids by inducing physical and chemical changes at pressures below the equilibrium transition thresholds. SHI irradiation not only drives physical phase transitions, as previously observed in ionic compounds,[5–7] but also induces chemical reactions in molecular solids, as evidenced by the polymerization of CO and the decomposition of urea. A key advantage of SHI irradiation compared with other techniques, such as laser heating or photoirradiation, is that the deposited energy density and thus the level of electronic excitation responsible for driving structural modifications, is extremely high and spatially confined to the nanoscale region surrounding the ion trajectories.[3–5] This method holds promise for the fabrication of two-phase composites mixed at the nanoscale, which is significant but difficult to achieve by other methods. Our findings reveal novel processes and provide new insights into the synergistic effects of SHI irradiation and high-pressure conditions in molecular systems. Future work combining *in situ* characterization and theoretical modeling will further elucidate the fundamental mechanisms driving these non-equilibrium transformations.

Author contributions

Jiaxu Liang: conceptualization, data curation, formal analysis, investigation, methodology, project administration, validation, visualization, writing – original draft, writing – review & editing; Lkhamsuren Bayarjargal: conceptualization, data curation, formal analysis, investigation, methodology, resources, supervision, validation, writing – original draft, writing – review & editing; Ioannis Tzifas: conceptualization, data curation, funding acquisition, methodology, project administration, resources, software, supervision, writing – original draft, writing – review & editing; Roman Belikov: data curation, investigation, writing – original draft, writing – review & editing; Lena Wedek: formal analysis, investigation, writing – original draft, writing – review & editing; Christopher Schröck: investigation, methodology, resources, software, writing – original draft, writing – review & editing; David Merges: methodology, resources, software, writing – original draft, writing – review & editing; Kay-Obbe Voss: data curation, investigation, methodology, resources, software, writing – original draft, writing – review & editing; Pascal Simon: data curation, investigation, methodology, resources, software, writing – original draft, writing – review & editing; Christina Trautmann: funding acquisition, methodology, project administration, resources, supervision, writing – original draft, writing – review & editing; Maria Toimil Molares: funding acquisition, methodology, project administration, resources, supervision, writing – original draft, writing - review & editing; Björn Winkler: conceptualization, funding acquisition, methodology, project administration, resources, supervision, writing – original draft, writing – review & editing.

Conflicts of interest

There are no conflicts to declare.

Data availability

The data supporting this article have been included as part of the supplementary information (SI). Supplementary information: experimental procedure, optical images, Raman/fluorescence spectra, and UV-Vis absorbance spectra. See DOI: https://doi.org/10.1039/d6cp00307a.

Acknowledgements

The project is funded by the program (grant no. 05K22RF3) of the German Federal Ministry of Education and Research (BMBF). L. B., L. W. and B. W. acknowledge the support from the DFG (WI1232 and BA4020). R. B. acknowledges the support from BMBF (grant no. 05P24RFB). C. S. acknowledges funding *via* the R&D program of GSI and support from the Helmholtz Graduate School HGS-HIRe. The results presented here are based on experiments performed at the SIS18 at the GSI Helmholtzzentrum für Schwerionenforschung, Darmstadt (Germany) in the frame of FAIR Phase-0.

References

1 M. Toulemonde, C. Dufour, Z. Wang and E. Paumier, *Nucl. Instrum. Methods Phys. Res., Sect. B*, 1996, **112**, 26–29.
2 M. Lang, F. Djurabekova, N. Medvedev, M. Toulemonde and C. Trautmann, *Comprehensive Nuclear Materials*, Elsevier, Oxford, 2nd edn, 2020, pp. 485–516.
3 M. Lang, R. Devanathan, M. Toulemonde and C. Trautmann, *Curr. Opin. Solid State Mater. Sci.*, 2015, **19**, 39–48.
4 A. P. Solomon, E. C. O'Quinn, J. Liu, I. M. Gussev, X. Guo, J. Neuefeind, C. Trautmann, R. C. Ewing, G. Baldinozzi and M. K. Lang, *Sci. Adv.*, 2025, **11**, eadq5943.
5 M. Lang, F. Zhang, J. Zhang, J. Wang, B. Schuster, C. Trautmann, R. Neumann, U. Becker and R. C. Ewing, *Nat. Mater.*, 2009, **8**, 793–797.
6 B. Schuster, F. Fujara, B. Merk, R. Neumann, T. Seidl and C. Trautmann, *Nucl. Instrum. Methods Phys. Res., Sect. B*, 2012, **277**, 45–52.
7 U. A. Glasmacher, M. Lang, H. Keppler, F. Langenhorst, R. Neumann, D. Schardt, C. Trautmann and G. A. Wagner, *Phys. Rev. Lett.*, 2006, **96**, 195701.
8 R. J. Hemley, *Annu. Rev. Phys. Chem.*, 2000, **51**, 763–800.
9 P. F. McMillan, *Chem. Soc. Rev.*, 2006, **35**, 855.
10 I. Tzifas, K.-O. Voss1, C. Schröck, P. Simon, J. Liang, L. Bayarjargal, M. Lang, R. Boehler, D. Merges, L. Kirsch, E. Zeqo, B. Winkler, M. E. Toimil-Molares and C. Trautmann, submitted, 2025, pp. 1–14.
11 M. J. Lipp, W. J. Evans, B. J. Baer and C.-S. Yoo, *Nat. Mater.*, 2005, **4**, 211–215.
12 R. L. Mills, B. Olinger and D. T. Cromer, *J. Chem. Phys.*, 1986, **84**, 2837–2845.
13 W. J. Evans, M. J. Lipp, C.-S. Yoo, H. Cynn, J. L. Herberg, R. S. Maxwell and M. F. Nicol, *Chem. Mater.*, 2006, **18**, 2520–2531.
14 N. Rademacher, L. Bayarjargal, W. Morgenroth, B. Winkler, J. Ciezak-Jenkins, I. G. Batyrev and V. Milman, *Chem. – Eur. J.*, 2014, **20**, 11531–11539.
15 S. Fang, H.-A. Ma, L.-S. Guo, L.-C. Chen, Y. Wang, L.-Y. Ding, Z.-H. Cai, J. Wang and X.-P. Jia, *Chin. Phys. B*, 2019, **28**, 098101.
16 F. J. Lamelas, Z. A. Dreger and Y. M. Gupta, *J. Phys. Chem. B*, 2005, **109**, 8206–8215.
17 K. Dziubek, M. Citroni, S. Fanetti, A. B. Cairns and R. Bini, *J. Phys. Chem. C*, 2017, **121**, 2380–2387.
18 F. Safari, M. Tkacz and A. Katrusiak, *J. Phys. Chem. C*, 2021, **125**, 7756–7762.
19 A. Abdulkarim, F. Hinkel, D. Jänsch, J. Freudenberg, F. E. Golling and K. Müllen, *J. Am. Chem. Soc.*, 2016, **138**, 16208–16211.
20 V. Strauss, H. Wang, S. Delacroix, M. Ledendecker and P. Wessig, *Chem. Sci.*, 2020, **11**, 8256–8266.
21 K. Shi, B. Liu, Y. Wu, Z. Liang, X. Wang, L. Su, Y. Wang, L. Zhang, G. Yang, Y. Zhang, C. Xie and Z. Zhao, *J. Phys. Chem. C*, 2019, **123**, 14696–14700.
22 K. Shi, X. Dong, Z. Zhao, L. Su, C. Ji, B. Li, J. Zhang, X. Dong, P. Qiao, X. Zhang, H. Yang, G. Yang, E. Gregoryanz and H.-K. Mao, *Nat. Commun.*, 2025, **16**, 357.
23 B. Eckert, H. O. Albert, H. J. Jodl and P. Foggi, *J. Phys. Chem.*, 1996, **100**, 8212–8219.
24 B. Eckert, R. Schumacher, H. J. Jodl and P. Foggi, *High Pressure Res.*, 2000, **17**, 113–146.
25 L. Chen, K. Shi, L. Su, S. Wang and G. Yang, *J. Photochem. Photobiol., A*, 2022, **430**, 113964.
26 A. G. Kalampounias, K. S. Andrikopoulos and S. N. Yannopoulos, *J. Chem. Phys.*, 2003, **118**, 8460–8467.
27 C.-S. Yoo, *Matter Radiat. Extremes*, 2020, **5**, 018202.